Inverse Resolution of the Heat-Transfer Equation: Application to Steel and Aluminum Alloy Quenching

P. Archambault and A. Azim

Two applications of the numerical method for the inverse heat conduction problem are presented. This numerical method calculates the surface temperature and heat flux using an internal experimental temperature evolution. In the case of aluminum alloys, the question of stability and sensitivity to error measurements is investigated and applied to actual quench cooling. For steel application (high heating and cooling rates), a new calculation procedure is developed to solve the problem of solution stability due to the nonmonotonous initial temperature profile generated by the superficial heating. This new calculation procedure allows the martensite tempered zones to be explained and localized.

Keywords

interrupted quench; quenching, aluminum; quench-heat transfer; quench modeling

1. Introduction

QUENCHING is one of the most critical operations in the heat treatment of many metallic parts, affecting both mechanical and structural properties. These effects are related to the quench cooling rate and to the instantaneous temperature gradients between the surface and the core of the part.

In the case of aluminum alloys, optimum quench cooling can be calculated on a metallurgical and a mechanical basis (solid-solution supersaturation and thermal deformations) (Ref 1). The practical realization of such a theoretical cooling is then possible (real-time controlled process) (Ref 2).

The heat treatment of steels can lead to complex experimental and metallurgical situations, especially in the case of superficial treating. These types of treatments are designed to obtain specific usage properties at the surface of the parts, which requires different metallurgical paths at the surface and in the bulk of the treated part (Ref 3).

In both cases and from an experimental point of view, the real surface temperature and heat flux remain unknown, as they cannot be measured. However, they are needed to determine the entire thermal and mechanical fields in the treated part and the mechanical and metallurgical paths of the superficial zone.

This paper describes the numerical method used to solve this typical inverse heat-conduction problem and its applications to steel and 7*xxx* aluminum alloy quenching.

2. Problem Formulation

Consider an infinite cylinder (no heat flux along the z axis) initially at a uniform temperature, T_0. During cooling, the heat-conduction transfer is governed by:

$$\rho C_p \delta T/\delta t = \text{div}[\lambda \, \text{grad}(T)] \qquad \text{(Eq 1)}$$

where T is temperature, ρ is density, C_p is specific heat, and λ is thermal conductivity. The thermophysical properties are considered to be dependent on temperature.

The initial and limit conditions are:

for $t = 0$	$T(r,0) = T_0$		
for $t > 0$	at $r = 0$	$(\delta T/\delta r)_{r=0} = 0$	
	at $r = r_e$	$T(r_e,t) = T_e(t)$	(measured)
	at $r = R$	$q = -\lambda \, (\delta T/\delta r)_{r=R}$	(unknown; to be estimated)

where q is surface heat flux, R is the radius of the cylinder, and r_e is the radial distance to where temperature is measured.

The temperature evolution at $r = r_e$ is supposed to be known (experimental measurement). It is then desired to predict the heat flux and the temperature evolutions at $r = R$ (cylinder surface). Thus, the entire domain can be divided into a direct region (between $r = 0$ and $r = r_e$) and an inverse region (between $r = r_e$ and $r = R$). In the direct region, the boundary conditions are known. It is then possible to solve easily this well-posed problem. The whole temperature-field calculation in this region is first computed independently of the inverse region and provides the needed data for the calculation in the inverse region, which is the second step of the global calculation. The following description and discussions concern only the inverse region, assuming that the calculations in the direct domain have already been performed.

2.1 *Temperature-Field Calculation*

In the inverse region, the heat-flow equation is discretized using an implicit finite-differences method (Ref 4). Then, Eq 1 can be written as:

$$a_i T_{i-1}^j + b_i T_i^j + c_i T_{i+1}^j = T_i^{j-1} \qquad \text{(Eq 2)}$$

where i is the index space, j is the index time, and:

P. Archambault, Laboratoire de Science et Génie des Matériaux Métalliques (LSG2M, URA CNRS 159), Ecole Des Mines, Parc de Saurupt, 54042 Nancy, France; **A. Azim,** Université Chouaib Doukkali, Faculté des Sciences, Département de Physique, BP 20 El-Jadida, Morocco.

$$a_i = -\alpha(T_{i-1}^{j-1})\frac{\Delta t}{\Delta r^2}\left[1 - \frac{1}{2(i-1)}\right]$$

$$c_i = -\alpha(T_{i+1}^{j-1})\frac{\Delta t}{\Delta r^2}\left[1 + \frac{1}{2(i-1)}\right]$$

$$b_i = 2\alpha(T_i^{j-1})\frac{\Delta t}{\Delta r^2} + 1$$

This leads to:

$$T_{i+1}^{j} = \frac{1}{c_i}T_i^{j-1} - \frac{a_i}{c_i}T_{i-1}^{j} - \frac{b_i}{c_i}T_i^{j} \qquad \text{(Eq 3)}$$

The temperature calculation at node $(e + 1,1)$ is possible because it uses known temperatures at nodes $(e - 1,1)$, $(e,1)$ and $(e,0)$. The temperature of the subsequent nodes is then calculated progressively toward the surface. At the end of the calculation, the temperature field between $r = r_e$ and $r = R$ is obtained for each step of time. These results are then used for calculating the evolution of the surface heat flux.

2.2 *Heat-Flux Calculation*

The heat-flux calculation uses the method described by Raynaud and Bransier (Ref 5). For a cylindrical geometry, the surface heat flux can then be written as:

$$q_M^j = \frac{1}{2\gamma}\left[(1-\alpha)\,T_M^{j+1} - (1+\beta)\,T_M^{j-1} + \alpha\,T_{M-1}^{j+1} + \beta\,T_{M-1}^{j-1}\right] \qquad \text{(Eq 4)}$$

where:

$$\alpha = \left[1 - \frac{1}{2(M-1)}\right]\lambda_{i-1/2}^{j+1}\left(\frac{\Delta t}{\Delta r^2 \rho C_p}\right)$$

$$\beta = \left[1 - \frac{1}{2(M-1)}\right]\lambda_{i-1/2}^{j-1}\left(\frac{\Delta t}{\Delta r^2 \rho C_p}\right)$$

$$\gamma = \left(1 + \frac{1}{2(M-1)}\right)\frac{\Delta t}{\Delta r\,\rho C_p}$$

Notice that the surface heat-flux calculation, at index time j, uses two future temperatures at nodes M and M – 1 (index time j + 1) and two past temperatures at nodes M and M – 1 (index time j – 1). This explicit algorithm starts at j = 1 (initial temperature distribution) and progresses with varying index j until j = *N* (final temperature distribution).

3. Application to Aluminum Alloy Quenching

For the alloy under consideration, the main input data are the variations of the thermophysical properties with temperature. Table 1 gives expressions for density, specific heat, and thermal conductivity temperature variations for 7*xxx* aluminum alloys (Ref 6).

3.1 *Validation of the Inverse Method*

In order to validate the inverse heat-conduction method, we have chosen the following test case: For a given heat-flux evolution, the temperature evolution at location $r = r_e$ is calculated using the direct method. This temperature evolution becomes the "experimental" cooling law of the inverse method, with which the corresponding surface heat-flux evolution is then recalculated.

From a numerical point of view, the choice of the time and space parameters is the most delicate operation in this algorithm. The Δt and Δr steps must be chosen carefully in order to increase the stability and the precision of the calculations. Thus, we have first fixed Δr (0.5 mm) and calculated the heat-flux evolution for several Δt values. The results are shown in Fig. 1 and reveal that, for a given Δr, the amplitude of the oscillations decreases with increasing time step. However, when the stability condition is satisfied ($\alpha\Delta t/\Delta r^2 > 1/2$), increasing Δt can be accompanied by a decreasing precision of the heat-flux calculations.

Figure 2 shows the heat-flux curves obtained for a fixed Δt (0.001 s) and several Δr values. It should be noted that, for $\Delta r = 0.5$ mm, some oscillations appear, the magnitude of which is significantly reduced with $\Delta r = 0.05$ mm. However, for the lower Δr (0.025 mm), instabilities arise again even though the stability condition is satisfied. This must be attributed to unavoidable truncating errors due to the numerous numerical operations.

We have also tested the algorithm behavior response to noisy data. This has shown that an experimental "noisy" temperature evolution with a maximum noise of 2 °C has no significant effect on the surface temperature calculation. (The maximal observed deviation with nonperturbated data is around 5 °C.)

3.2 *Application to an Actual Quench Cooling Case*

In an earlier study (Ref 7) dealing with the optimization of aluminum alloy quenching (high mechanical properties associated with low deformations and stresses), an optimum quench cooling that presents an accelerated kinetic was calculated. This result and its mechanical consequences had to be verified experimentally. Because such a temperature evolution is not attainable with classical immersion quenching, a real-time controlled water-spraying system developed at the Laboratoire de Science et Génie des Matériaux Métalliques was used to apply this

Table 1 Thermophysical properties of 7*xxx* aluminum alloys

ρ, kg/m^3	2700
C_p, J/kg · °C	$820 + 0.77T$
λ, W/m · °C	$111 + 194 \times 10^{-3}\,T - 210 \times 10^{-6}\,T^2 + 90 \times 10^{-9}\,T^3$

calculated optimum cooling to cylinders of 7475 alloy (20 mm diam) (Ref 1). The temperature control was performed with the aid of a thermocouple located beneath the surface of the sample ($r_e = 9$ mm). After quenching, the surface residual stresses were measured by x-ray diffraction (XRD) analysis (Ref 7).

In order to calculate the real evolution of deformations and stresses appearing in the sample during cooling, the entire temperature field in the cylinder and thus the variation of the surface heat flux with temperature had to be determined. The experimental temperature evolution at $r = r_e$ is used in the inverse algorithm to determine the surface heat-flux variation with temperature. This is then used as input data in a thermoelastoplastic finite-element code (Ref 8) for calculating the residual stresses at the end of cooling. Figure 3 shows the surface temperature and the heat-flux evolution calculated by the inverse method. The shape of the temperature curve corresponds to the "accelerated" cooling. Around 250 °C, the heat-flux evolution is due to the wetting of the surface of the sample as experimentally registered at $r = r_e$.

Using this quite realistic heat flux evolution, we have then calculated the residual tangential stress radial profile presented in Fig. 4. Due to the optimization of the cooling, the stress is null along the radius except just beneath the surface, where one can observe a very good agreement with the value obtained by XRD ($\sigma = -28 \pm 3$ MPa). This clearly indicates that the inverse method developed in this study yields accurate and reliable results, which should allow estimation of quench cooling parameters and consequences that are not experimentally attainable.

4. Application to Steel Quenching

4.1 *Experimental Context*

Another earlier study by the authors concerned optimization of the superficial heat treatment of steel parts in order to produce a hard homogeneous surface layer over a more ductile

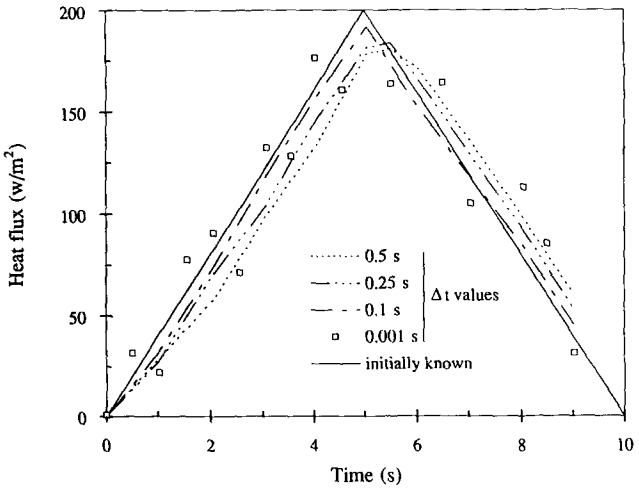

Fig. 1 Inverse method stability: influence of time step Δt for a given Δr (0.5 mm)

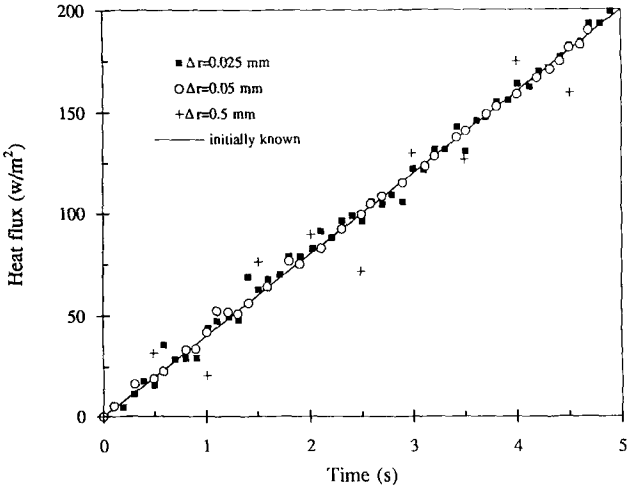

Fig. 2 Inverse method stability: influence of space step Δr for a given Δt (0.001 s)

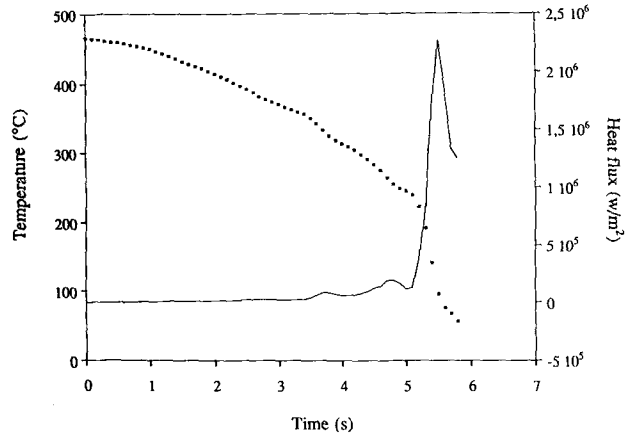

Fig. 3 Calculated surface temperature and heat-flux evolutions. M = 21, $\Delta t = 0.1$ s, $\Delta r = 0.5$ mm

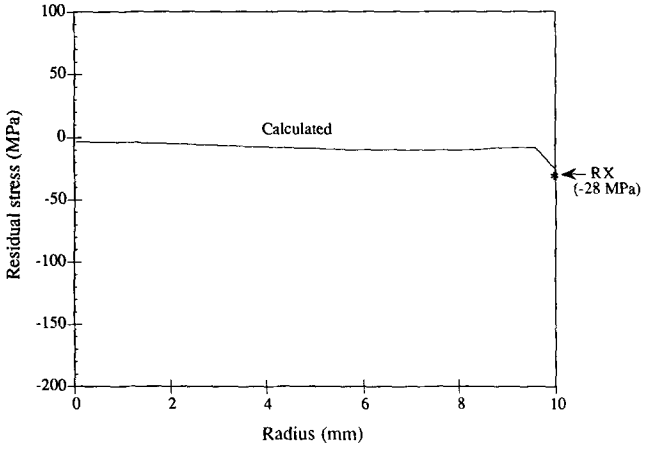

Fig. 4 Calculated radial profile of the tangential residual stress (20 mm diam 7475 alloy). Superficial stress measured by XRD.

bulk. This was achieved by means of fast heating (200 °C/s), followed by fast cooling (200 °C/s) interrupted at a given temperature by an isothermal holding above M_s (superficial temperature "homogenization" before martensitic transformation). After 10 s of holding (T = 480 °C), the sample was then cooled to room temperature for martensitic transformation. Induction heating associated with the real-time controlled water-spraying system was used for cooling (Ref 2, 9). The sample was a 16 mm diam, 30 mm long cylinder; the temperature (for process control) was measured at 1.5 mm beneath the surface of the cylinder. The high heating rate promoted a high radial temperature gradient as measured just before cooling (Fig. 5). This revealed that only a superficial zone is austenitic at the end of the heating and is subsequently transformed to martensite at the end of cooling.

After heat treating, metallurgical examination of the sample (microstructure and hardness) (Fig. 6) revealed a low hardness due to the tempered martensite arising at the surface of the sample (Ref 10). This seemed to indicate that the temperature of the superficial zone (between the measurement location and the surface) was not perfectly controlled and came below M_s just before isothermal holding because of the high cooling rate. In order to verify this hypothesis and improve the thermal control process, we had to determine the superficial thermal field developed during cooling.

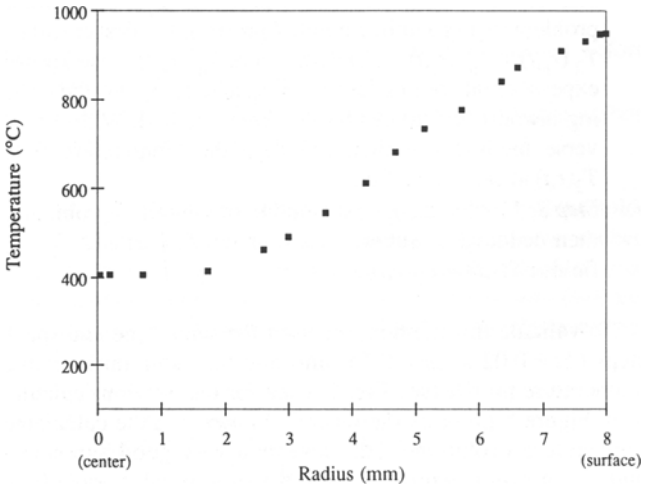

Fig. 5 Experimental radial temperature profile reached at the end of heating (just before the cooling process)

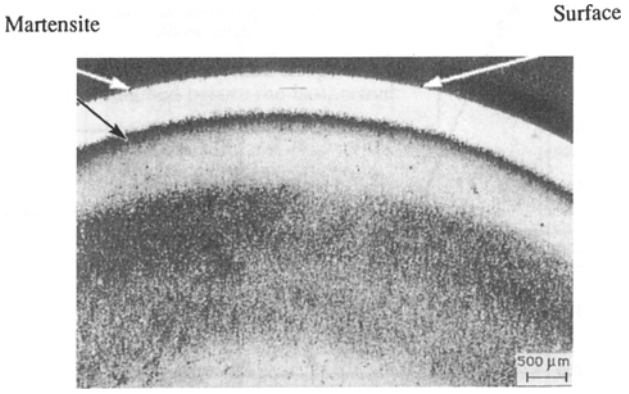

(a)

4.2 *Algorithm and Numerical Validation*

We first used the previously described numerical procedure with minor adaptations:

- The initial temperature boundary condition becomes nonmonotonous; thus, $T(r,0) = f(r)$.
- The thermophysical properties are that of a carbon steel (Table 2).

To validate this calculation in that particular case before any application to the real heat treatment, we performed the following test: For a given "fictitious" temperature evolution, the temperature evolution at $r = r_e$ was calculated using the direct method. This calculated evolution became the "experimental" cooling law of the present inverse method, with which the surface temperature evolution was then calculated and compared with the initial "fictitious" one. The results are presented in Fig. 7 for two cases (Δt = 0.02 and 0.05 s; Δr = 0.15 mm). They show clearly a bad estimation of the surface temperature evolution when the initial temperature profile is nonmonotonous. To solve this difficulty, we have developed a new calculation procedure that consists of dividing the initial problem into two elementary parts.

Table 2 Thermophysical properties of carbon steel

ρ, kg/m^3	7760
C_p, J/kg · °C	$4.5 \times 10^{-4}\ T^2 + 0.084T + 475.7$
λ, W/m · °C	$-1.94 \times 10^{-5}\ T^2 - 9.36 \times 10^{-3}\ T + 46.76$

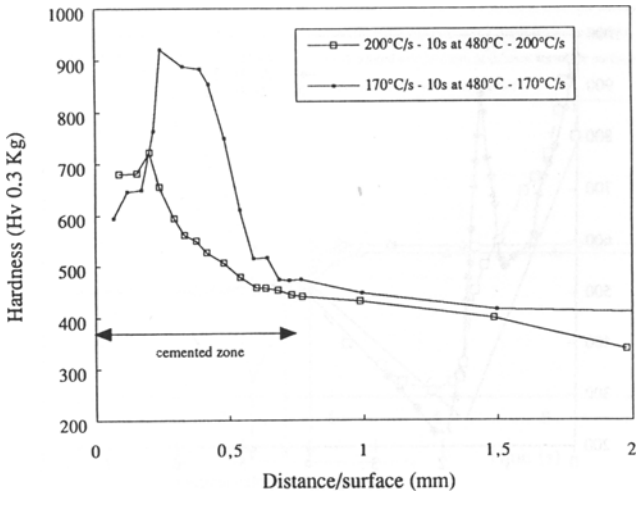

(b)

Fig. 6 (a) Micrograph of the cemented zone (170 °C/s for 10 s at 480 °C – 170 °C/s). (b) Hardness profile in the cemented zone (170 and 200 °C/s)

Initial problem:

$$\frac{1}{r}\frac{\partial T}{\partial r}+\frac{\partial^2 T}{\partial r^2}=\frac{1}{\alpha}\frac{\partial T}{\partial t} \qquad \alpha=\frac{\lambda}{\rho C_p}=f(T)$$

at $t=0$ $\quad T(r,0)=T_i(r)$ (nonmonotonous initial temperature profile)

$$t>0 \begin{cases} \left[\frac{\partial T}{\partial r}\right]_{r=0}=0 \\ T(R,t)=T_s(t) \text{ (unknown) (surface temperature)} \\ T(r_e,t)=T_m(t) \text{ (experimental cooling law at } r=r_e) \end{cases}$$

Elementary problem 1—direct with a nonmonotonous initial radial profile:

$$\frac{1}{r}\frac{\partial T_1}{\partial r}+\frac{\partial^2 T_1}{\partial r^2}=\frac{1}{\alpha}\frac{\partial T_1}{\partial t}$$

at $t=0$ $\quad T_1(r,0)=T_i(r)-T_s(0)=T_i(r)-T_i(R)$

$$t>0 \quad \left[\frac{\partial T_1}{\partial r}\right]_{r=0}=0$$

$$T_1(R,t)=0$$

Elementary problem 2—inverse with a uniform initial radial profile:

$$\frac{1}{r}\frac{\partial T_2}{\partial r}+\frac{\partial^2 T_2}{\partial r^2}=\frac{1}{\alpha}\frac{\partial T_2}{\partial t}$$

at $t=0$ $\quad T_2(r,0)=T_s(0)=T_i(R)$

$$t>0 \quad \left[\frac{\partial T_2}{\partial r}\right]_{r=0}=0$$

$$T_2(R,t)=T_s(t) \text{ (unknown)}$$

$$T_2(r_e,t)=T_m(r_e,t)-T_1(r_e,t)$$

- *Step 1:* The first elementary problem (T_1) is resolved by a direct method (using a nonuniform initial profile) for calculating $T_1(r,t)$ and particularly $T_1(r_e,t)$, where r_e is the radial position of the known experimental cooling law in the initial problem.
- *Step 2:* The second elementary problem (T_2) is an inverse problem (using a uniform initial profile). We first calculate $T_2(r_e,t)=T_m(r_e,t)-T_1(r_e,t)$, where $T_m(r_e,t)$ is the known experimental cooling law at $r=r_e$, and $T_1(r_e,t)$ is the cooling law at r_e calculated by the direct method. With the inverse method, we then calculate the temperature field $T_2(r,t)$ at each step of time.
- *Step 3:* Finally, the global solution of the initial problem is then deduced by superposition of the $T_1(r,t)$ and $T_2(r,t)$ fields: $T(r,t)=T_1(r,t)+T_2(r,t)$.

To validate this method, we used the same time and space steps ($\Delta t=0.02$ s, $\Delta r=0.15$ mm) and the same initial radial temperature profile (see Fig. 5) used for the previous calculation. Figure 8 presents the initially known and the calculated temperature evolutions. This reveals a very good agreement and thus a major improvement in the superficial thermal field calculation.

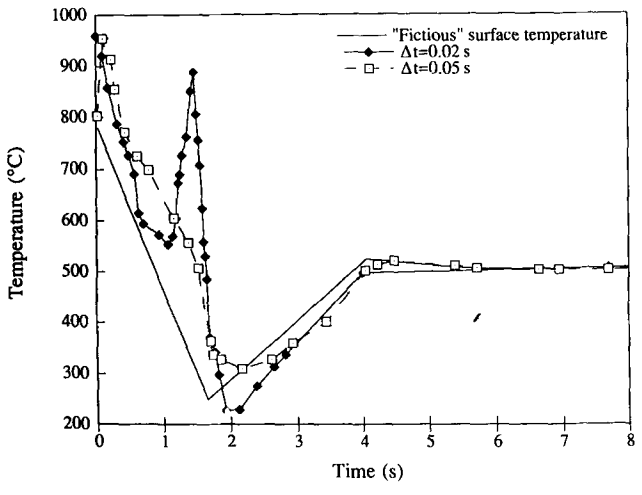

Fig. 7 Inverse method application using nonmonotonous profile. $\Delta r=0.15$ mm, $\Delta t=0.05$ s, $\Delta t=0.02$ s

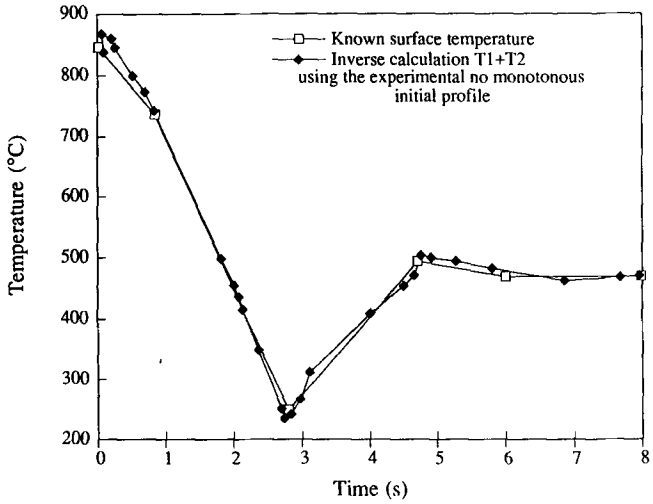

Fig. 8 Validation of the new inverse calculation methodology. $\Delta r=0.15$ mm, $\Delta t=0.02$ s

4.3 *Application to an Actual Heat Treatment*

In order to validate our metallurgical hypothesis, we have adopted the procedure presented in Fig. 9. Using the new calculation method (see section 4.2) and for the given experimental cooling law registered at 1.5 mm beneath the surface, we calculated the temperature evolutions $T = f(t)$ at different locations in the superficial zone and deduced the lowest temperatures reached before the isothermal holding.

Figure 10 shows the experimental and calculated cooling evolutions for an actual heat-treating case (cemented steel). One can see that the experimental cooling is perfectly controlled, but, due to the high cooling rate, the temperature of the superficial zone quickly becomes lower than the holding temperature during the first step of the cooling. We can now compare the minimal temperatures reached before the holding with the corresponding M_s temperatures measured elsewhere for the studied steels (Ref 10) and quantify the deviation between the temperature reached in the superficial zone and the M_s temperature. For the region between the surface of the sample and the temperature measurement location (1.5 mm), Fig. 11 shows:

- The profile of the minimal temperature reached before holdings at 330, 480, and 560 °C
- The variation of the M_s temperature related to the carbon profile after cementation

These results indicate that when the temperature of the holding is high enough (560 °C), the minimal temperatures reached just before the isothermal holding are not low enough to promote martensitic transformation. For the two other cases (480 and 330 °C), the temperature before the holding can effectively become lower than the M_s temperature. The martensite thus formed can then be tempered because of reheating (by internal conduction) to the holding temperature when this is higher than M_s.

The structural anomalies (low hardness zones) observed experimentally are thus due to this complex thermal and metallurgical interaction (Ref 10). This means that for such fast heat treatments, our temperature-controlling process was not reliable enough to ensure precise superficial metallurgical paths. This has been modified for controlling the real surface temperature by means of infrared sensors. This noncontact solution led to coherent thermal and metallurgical results (to be published).

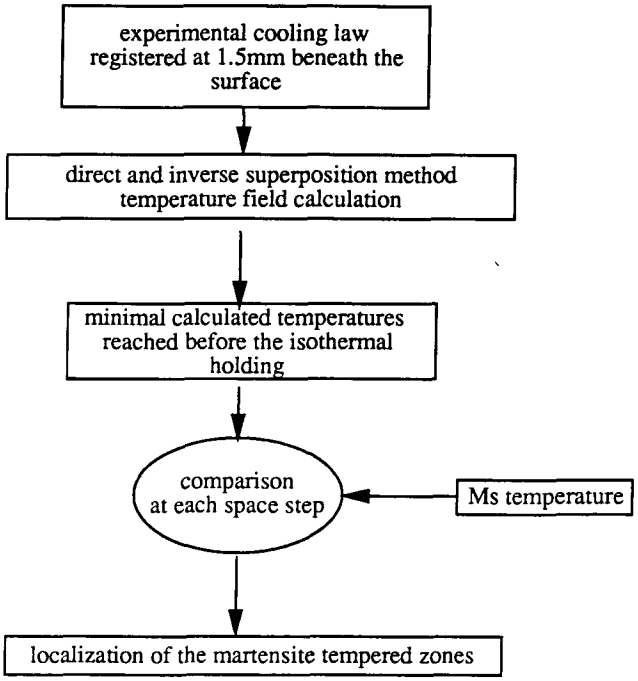

Fig. 9 Procedure used for illustrating the structural anomalies in superficial zones

5. Conclusions

A numerical technique for the solution of a nonlinear inverse heat-conduction problem has been presented for calculating the surface temperature and heat flux in a cylindrical geometry. The question of stability and sensitivity to error measurements has been investigated. It was shown by a set of examples that stability is ensured by an adequate choice of space and time steps and that sensitivity to error measurements is quite limited.

The algorithm described in this paper has been used (1) to study the quenching of aluminum alloys for which the phase transformations do not involve a significant thermal internal source (low volume fraction of precipitation) and (2) to explain metallurgical anomalies observed after superficial quenching of steels. The main difficulty in this last case was to take into account the nonuniform initial temperature due to the high heating rate (superficial heat treatment). This problem was solved by using a superposition algorithm involving two parts: direct (shifted nonuniform initial profile) and inverse (constant initial temperature).

For aluminum alloys, the presented method allowed validation of the optimum quench cooling concept (high supersaturation associated with no residual stresses). The results obtained

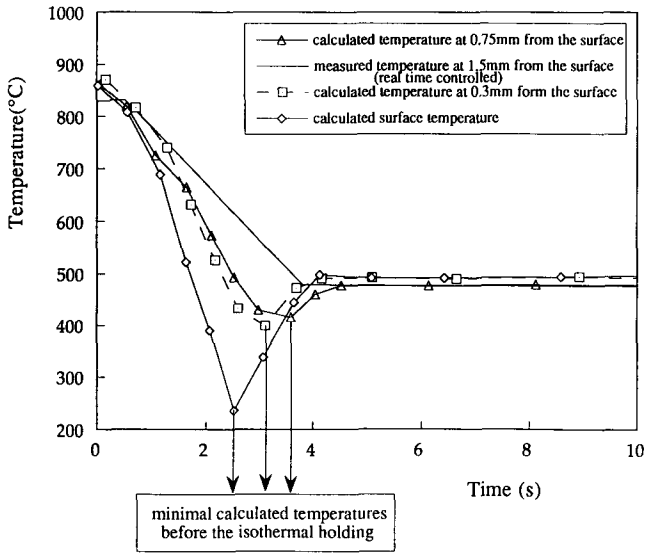

Fig. 10 Calculated cooling evolutions for the actual heat treating of cemented steel

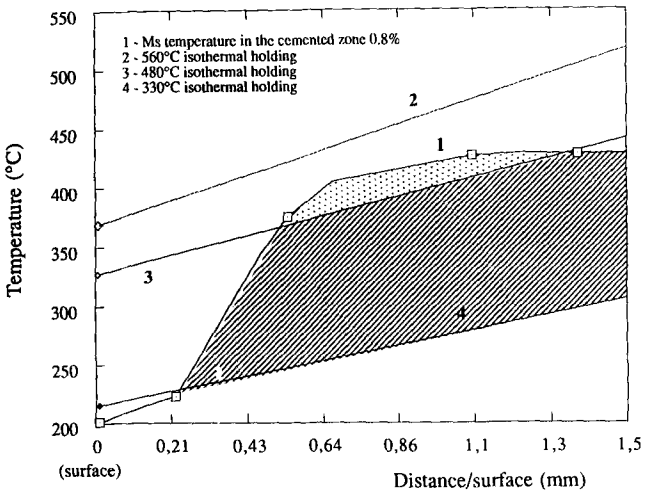

Fig. 11 Comparison between the minimal and M_S temperatures reached before the isothermal holding (cemented sample)

for interrupted cooling of steel have confirmed and improved the metallurgical hypothesis. Due to a high cooling rate before isothermal holding above the martensitic transformation temperature, the temperature of the superficial zone can become lower than M_S, promoting a localized transformation followed by tempering.

This work is continuing to investigate more complex cases in order to take into account the internal thermal source and the variations of the thermal properties due to the metallurgical transformations induced by the temperature variation (heating and cooling).

References

1. A. Azim and P. Archambault, "Quench Cooling Optimization for Aluminum Alloys," presented at Int. Conf. Residual Stresses (Nancy, France), 1989
2. P. Archambault, G. Didier, F. Moreaux, and G. Beck, Computer Controlled Spray Quenching, *Met. Prog.*, Vol 126 (No. 5), Oct 1984, p 67-72
3. P. Archambault, M. Pierronnet, F. Moreaux, and Y. Pourprix, in *Proc. 1st ASM Heat Treatment and Surface Engineering Conference and Exhibition*, Trans Tech, 1991, p 335-343
4. A. Azim, Optimisation du Refroidissement de Trempe d'Alliages à Base d'Aluminium: Recherche Numérique et Caractérisation Expérimentale, Thèse ès sciences, Institut National Polytechnique De Lorraine, Nancy, France, June 1989 (in French)
5. M. Raynaud and P. Bransier, Experimental Validation of New Space Matching Finite Difference Algorithm for the Inverse Heat Conduction Problem, *Proc. 8th Int. Heat Transfer Conf.*, Hemisphere Publishing Corporation, NY, 1986, p 17-22
6. J.E. Hatch, *Aluminum—Properties and Physical Metallurgy*, ASM International, 1984
7. A. Azim and P. Archambault, "Optimum Quench Cooling for Aluminum Alloys. Calculated and Experimental Results," presented at International Congress on Heat Treatment of Materials (Chicago), 28-30 Sept 1988
8. S. Denis, Modélisation des Interactions Contrainte-Transformation de Phase et Calcul par Éléments Finis la Genèse des Contraintes Internes au Cours de la Trempe des Aciers, Thèse ès sciences, Institut National Polytechnique De Lorraine, Nancy, France, 1987 (in French)
9. P. Archambault and F. Moreaux, "Traitement Thermique Superficiel par Induction: Chauffage et Refroidissement Pilotés en Temps Réel," presented at MAT-TEC 90 (Grenoble, France), 15-19 Oct 1990 (in French)
10. M. Pierronnet, P. Archambault, F. Moreaux, B. Clement, and M. Beauget, Comportement Métallurgique et Mécanique d'Aciers Trempés par Induction après Cémentation, *Trait. Therm.*, Vol 222, 1988, p 35-41 (in French)